RECOVERY OF 29-s OSCILLATIONS IN HST/FOS ECLIPSE OBSERVATIONS OF THE CATACLYSMIC VARIABLE UX Ursae Majoris[1]

Christian Knigge
Space Telescope Science Institute
3700 San Martin Drive, Baltimore, MD 21218, knigge@stsci.edu

Nick Drake
The University of Southampton, Department of Physics & Astronomy
Southampton SO17 1BJ, United Kingdom, nsd@astro.soton.ac.uk

Knox S. Long
Space Telescope Science Institute
3700 San Martin Drive, Baltimore, MD 21218, long@stsci.edu

Richard A. Wade
The Pennsylvania State University, Department of Astronomy and Astrophysics
525 Davey Laboratory, University Park, PA 16802, wade@astro.psu.edu

Keith Horne
Department of Physics and Astronomy, The University of St. Andrews
North Haugh, St. Andrews, Fife, KY16 9SS, UK, kdh1@st-andrews.ac.uk

Raymundo Baptista
Departamento de Fisica, Universidade Federal de Santa Catarina
Campus Universitario, Trindade, 88040 Florianopolis, Brasil, bap@fsc.ufsc.br

To be published in the *The Astrophysical Journal*

Received 6 August 1997 ; Accepted 25 November 1997

[1]Based on observations with the NASA/ESA *Hubble Space Telescope*, obtained at the Space Telescope Science Institute, which is operated by the Association of Universities for Research in Astronomy, Inc., under NASA contract NAS 5-2655.

ABSTRACT

Low amplitude ($\simeq 0.5\%$) 29-s oscillations have been detected in HST/FOS eclipse observations of the nova-like cataclysmic variable UX UMa. These are the same dwarf nova-type oscillations that were originally discovered in this system by Warner & Nather in 1972. The 29-s oscillations are seen in one pair of eclipse sequences obtained with the FOS/PRISM in November of 1994, but not in a similar pair obtained with the FOS/G160L grating in August of the same year. The oscillations in the PRISM data are sinusoidal to within the small observational errors and undergo an approximately -360^{o} phase shift during eclipses (i.e., one cycle is lost). Their amplitudes are highest at pre-eclipse orbital phases and exhibit a rather gradual eclipse whose shape is roughly similar to, though perhaps slightly narrower than, UX UMa's overall light curve in the PRISM bandpass (2000 Å–8000 Å).

Spectra of the oscillations have been constructed from pre-, mid- and post-eclipse data segments of the November observations. The spectra obtained from the out-of-eclipse segments are extremely blue, and only lower limits can be placed on the temperature of the source which dominates the modulated flux at these orbital phases. Lower limits derived from blackbody (stellar atmosphere) model fits to these data are $\geq 95,000$ K ($\geq 85,000$ K); the corresponding upper limits on the projected area of this source are all $< 2\%$ of the WD surface area. By contrast, oscillation spectra derived from mid-eclipse data segments are much redder. Fits to these spectra yield temperature estimates in the range $20,000\ \mathrm{K} \lesssim T \lesssim 30,000$ K for both BB and SA models and corresponding projected areas of a few percent of the WD surface area. These estimates are subject to revision if the modulated emission is optically thin.

We suggest that the ultimate source of the oscillations is a hot, compact region near disk center, but that a significant fraction of the observed, modulated flux is due to reprocessing of the light emitted by this source in the accretion disk atmosphere. The compact source is occulted at orbital phases near mid-eclipse, leaving only part of the more extended reprocessing region(s) to produce the weak oscillations that persist even at conjunction.

The highly sinusoidal oscillation pulse shape does not permit the identification of the compact component in this model with emission produced by a rotating disturbance in the inner disk or in a classical, equatorial boundary layer. Instead, this component could arise in a bright spot on the surface of the WD, possibly associated with a magnetic pole. However, a standard intermediate polar model can also be ruled out, since UX UMa's oscillation period has been seen to change on time-scales much shorter than the minimum time-scale required to spin up the WD by accretion torques. A model invoking magnetically controlled accretion onto *differentially rotating* WD surface layers may be viable, but needs more theoretical work.

1. INTRODUCTION

Cataclysmic variable stars (CVs) are semi-detached binary systems in which mass is transferred from a Roche lobe-filling, approximately main-sequence secondary onto an accretion disk around a mass-gaining white dwarf (WD) primary. In the nova-like (NL) CVs, the accretion disk is optically thick and dominates the ultraviolet (UV) and optical light. This makes NL CVs excellent targets for observational studies of accretion disk physics, particularly since their binary nature often allows their system parameters to be determined quite accurately,

In a previous paper (Knigge et al. 1997, hereafter Paper I), we presented a set of spectrally- and orbital phase-resolved eclipse observations of the NLCV UX UMa that were obtained with the *Faint Object Spectrograph* (FOS) onboard the *Hubble Space Telescope* (HST). In our analysis of the data in Paper I, the emphasis was on the spectral characteristics of the system components that could be isolated in the data (the accretion disk, the bright spot and the uneclipsed light). Here, we focus on UX UMa's 29-s oscillations which exist in some of our data. These oscillations were originally discovered in this system by Warner & Nather (1972, hereafter WN72) and belong to the class of "dwarf nova oscillations" (DNOs). The name derives from the fact that DNOs—small-amplitude ($\lesssim 0.5\%$), short-period ($7\ \mathrm{s} \lesssim P_{DNO} \lesssim 40\ \mathrm{s}$) and reasonably coherent ($10^4 \lesssim Q = |\dot{P_{DNO}}|^{-1} \lesssim 10^6$) oscillations—have been observed mainly in dwarf novae (DNe) in outburst, although a few other NLs also exhibit such modulations (e.g., Warner 1995). Most observations of DNOs have been at optical wavelengths, but some systems are known to show periodic x-ray oscillations as well. The very stable ($Q > 10^{12}$) oscillations displayed by two intermediate polars (IPs)—AE Aqr and DQ Her—may also be related to the DNO phenomenon.

The origin of DNOs is not certain. Two relatively plausible scenarios invoke magnetically controlled accretion close to the WD, and relatively long-lived disturbances in the inner disk or the boundary layer (see Warner 1995 for a recent review). In both models, the ultimate source of the oscillations is near the center of the accretion disk and the period of the oscillations is identified with the dynamical (rotational) time scale in the vicinity of the source. In fact, the latter identification is common to essentially all models for the origin of DNOs, mainly because all other time scales (e.g., thermal and viscous ones) are long compared to typical DNO periods (tens of seconds). Thus DNOs may be a unique probe of the physical conditions very close to the central source in those disk-accreting systems that exhibit these oscillations. Moreover, given the relative ubiquity of DNOs among CVs, their excitation mechanism is likely to be of quite general significance to our understanding of accretion disk physics.

The plan of this paper is as follows: in Section 2, we briefly describe the relevant aspects of the observations and their reduction. UX UMa's 29-s oscillations are then recovered and analyzed in Section 3. There we consider the eclipse behavior, mean pulse shape and coherence properties, as well as the spectrum of the oscillations. We discuss our results in Section 4, focusing particularly on the impact of our new data on models for the origin of DNOs. Finally, we present our conclusions in Section 5.

2. OBSERVATIONS

UX UMa was observed with the FOS on HST in August and November of 1994. Two eclipses were followed in each epoch. The two August eclipse observations (Runs 1 and 2) were carried out with the G160L grating and covered consecutive orbital cycles; the two November observations (Runs 3 and 4) were obtained with the PRISM and were separated by two unobserved eclipses. All observations were carried out in RAPID mode, with a new exposure beginning every 5.4 s.

The nominal wavelength coverages of the spectral elements used in the two observing epochs were 1140 Å–2508 Å (G160L; August) and 1850 Å–8950 Å (PRISM; November). However, for practical purposes (see Paper I), we restricted our analysis of the data to 1230 Å–2300 Å for G160L spectra and 2000 Å–8000 Å for PRISM spectra. The spectral resolution of the G160L was 6.6 Å FWHM with our instrumental set-up; that of the PRISM varied from a few Angstrom near the short wavelength end to a few hundred Angstrom near the long wavelength end. In observations with the G160L grating, the zeroth order light is also recorded and can be used to construct a broad-band optical/UV light curve. The zeroth order light has a bandpass with full-width at half-response of 1900 Å and a pivot wavelength of 3400 Å. For more details on the observations and their reduction, the reader is referred to Paper I.

In the top panels of Figure 1, "white-light" light curves are shown for the four observing runs. These have been constructed as time-series of the average flux across the full adopted wavelength range of the relevant dispersion element in each exposure. For the G160L observing sequences, the zeroth order time series are also shown. Note that UX UMa was $\sim 50\%$ brighter in November than in August, which, if due to a change in the accretion rate, indicates an increase in $\dot{M}_{acc}$ by $\gtrsim 50\%$ (Paper I).

Lomb-Scargle power spectra (Lomb 1976; Scargle 1982) calculated from these light curves are plotted in the bottom panels of Figure 1. Flickering—the non-periodic, intrinsic variability common to essentially all types of CVs—shows up in these power spectra as a general increase in power towards low frequencies. Peaks at frequencies corresponding to periods of about 29 s are nevertheless easily identified in the power spectra of Runs 3 and 4 (November; PRISM) since they are well separated from the low-frequency flickering-dominated regime. Similar peaks are not seen in any of the power spectra constructed for Runs 1 and 2 (August; G160L).

3. RECOVERY AND ANALYSIS OF THE 29-SECOND OSCILLATIONS

Before embarking on the analysis of the oscillations in our own data, we briefly review the more striking properties of the 29-s oscillations observed by WN72 and NR74. The oscillations analyzed by WN72 had an amplitude of about 0.002 mag

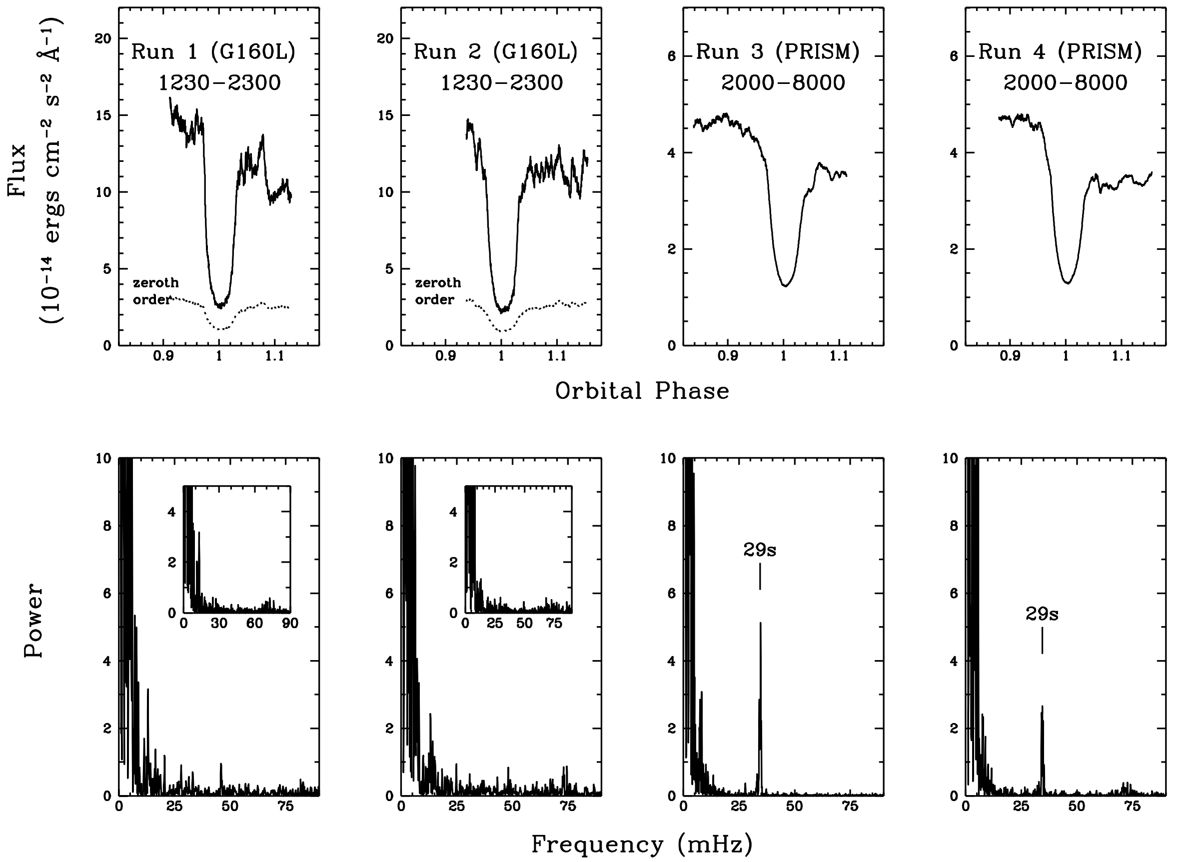

Fig. 1.— Light curves and power spectra constructed from the time-resolved HST/FOS spectra of UX UMa. *Top panels:* "White-light" (solid lines) and zeroth order (dashed lines; Runs 1 and 2 only) light curves phased according to the ephemeris of Baptista et al. (1995). The observing sequence corresponding to the light curve(s) in a given panel and the wavelength range over which the spectra have been averaged to produce the first-order light curve are indicated in each panel. See text for the calibration of the zeroth order G160L light curves. *Bottom panels:* Lomb-Scargle power spectra calculated from the the light curves shown in the corresponding top panels; to minimize the effects of the eclipses, light curves were divided by smoothed versions of themselves before calculating the power spectra.

(approximately 0.2%) in white optical light,[2] were detected at orbital phases before, during and after eclipse, and had a pulse shape that was sinusoidal to within observational uncertainties. In addition, WN72 found that the oscillations were not present in all of their observing runs, and that their period was slightly, but measurably different in the two runs in which they were detected. Finally, NR74 showed that the oscillations underwent a -360° phase shift (meaning that one oscillation cycle was lost) during eclipse, even though no obvious eclipse-related amplitude modulations were detected.

3.1. Wavelength-averaged Properties

Given this background, we decided to demodulate our time series using the "sliding sine fit" technique described by NR74. The first step in this procedure is to apply a high-pass filter to the light curves to remove long term trends. We filtered the data by subtracting a 5-point running mean from each datum in each time series. Given our time resolution of 5.4 s, a 5-point boxcar smoothing corresponds to averaging over about one 29-s oscillation cycle. We also experimented with an 11-point boxcar filter (corresponding to an average

[2]Throughout this paper, we will use the terms "peak-to-peak amplitude" and "amplitude" to denote the full peak-to-peak amplitude of a periodic signal and one half thereof, respectively.

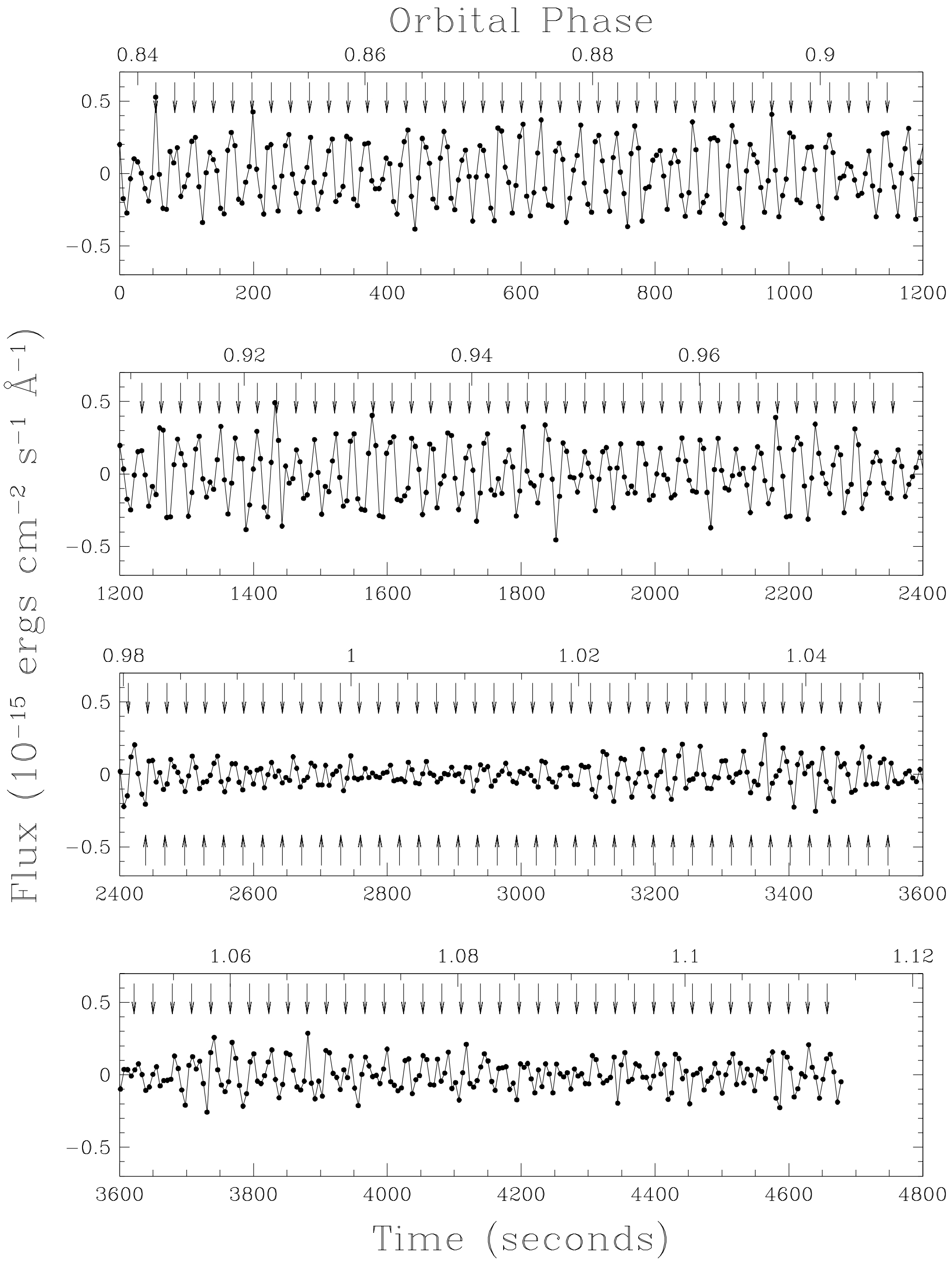

Fig. 2.— The high-pass filtered time series for Run 3. Shown is the white light (2000 Å–8000 Å) light curve for Run 3 after subtraction of a 5-point running mean, to reveal the small amplitude (approximately 0.5%) 29-s oscillations. The data are shown as a function of both time (in seconds; bottom x axes) and orbital phase (top x axes). The arrows above the data mark the times of maxima predicted from the peak in the pre-eclipse power spectrum after aligning to the first obvious observed maximum. The arrows below the data at phases close to conjunction (third panel from the top) mark the times of minima predicted from the mid-eclipse power spectrum after aligning to the first obvious observed minimum.

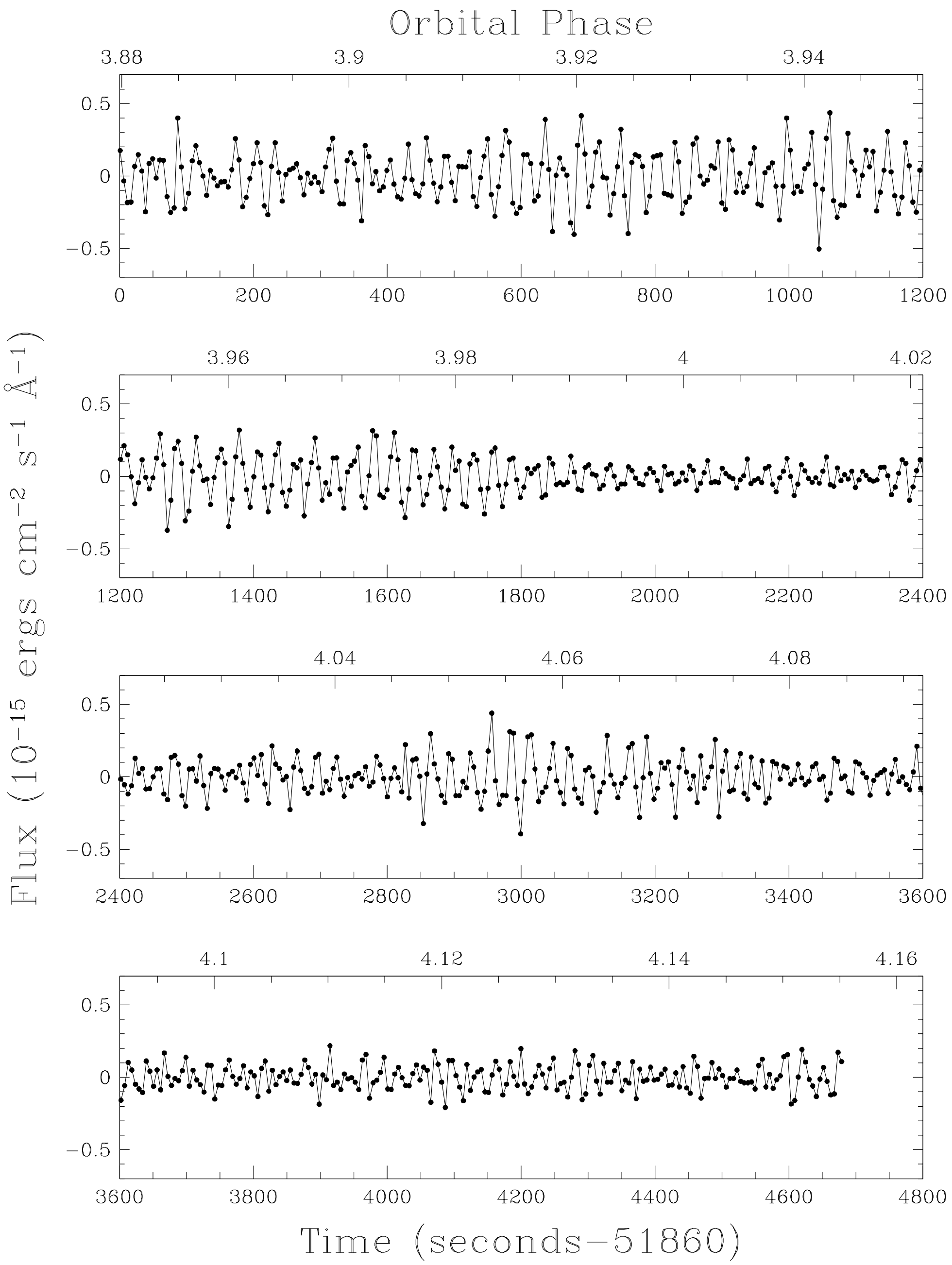

Fig. 3.— As Figure 2, but for the Run 4 data set.

over 2 oscillation cycles) and found that this gave essentially identical, but somewhat noisier results. The resulting high-pass filtered time-series are shown in Figures 2 and 3. The oscillations are seen clearly in the filtered data and appear to be approximately sinusoidal. In addition, there seems to be an eclipse-related decrease in the oscillation amplitudes.

Next, power spectra were calculated from the filtered data sets in order to identify the oscillation periods more accurately. These power spectra are shown in Figure 4, treating pre-, mid- and post-eclipse phases separately to avoid averaging over possible eclipse phase shifts. The appropriate periods to be used in demodulating the data are easily identified from the power spectra—they are the pre-eclipse periods of 28.77 s (Run 3) and 28.60 s (Run 4)—but a number of other points are also worth noting from this figure. First, the peak powers in all six power spectra are highly significant. This is immediately obvious from the high power levels in the Lomb-Scargle periodograms (in which power is normalized to the variance of the data) and supported by robust, distribution-free randomization tests we have carried out. Thus the 29-s oscillations are detected at all orbital phases, consistent with the results of WN72. Second, the peaks are highest in the power spectra calculated from the pre-eclipse data segments, suggesting that the amplitude of the oscillations was also highest there. This again gives hope that we may be able to detect and characterize amplitude variations as a function of orbital phase for the first time. Third, the power spectra suggest that the oscillation period at mid-eclipse orbital phases is slightly, but systematically lower than at pre- and post-eclipse phases. This is the first hint that we are seeing the eclipse phase shift described by NR74 in our data as well. (Note that if a time series is demodulated by fitting sinusoids with fixed period but variable phase, a linear phase shift indicates that the signal in the data repeats on a slightly different period than assumed in the fit.) Fourth, the periods detected in the pre-, mid- and post-eclipse time series are equal for both November observing runs, to within the uncertainties defined by the widths of the peaks in the power spectra. Fifth, the inset in Figure 4 shows that we do not detect any signal at the first overtone frequency in the power spectrum of the data segment in which the oscillations are detected most cleanly (Run 3 pre-eclipse). This gives quantitative support to the visual impression from Figures 2 and 3 that the oscillations are sinusoidal to high accuracy. To test for the presence of sub-harmonics, we have also inspected the power spectrum constructed from the Run 3 pre-eclipse light curve after filtering the data with several wider filters, ranging in width from 2 to 4 oscillation cycles. No power excesses were found at frequencies corresponding to integral multiples of the 29-s period.

The highly sinusoidal character of the oscillations is illustrated more directly in Figure 5. This shows the result of folding the Run 3 pre-eclipse, high pass-filtered time series onto the 28.77 s oscillation period and binning the resulting light curve into 20 non-overlapping phase bins. The figure establishes that the mean pulse shape is a simple sinusoid to within the small observational errors. This result is not an artifact of the narrow filter width used: a fixed-period sinusoid fit to the same data segment after applying a filter of twice the original width still gives an excellent reduced χ^2 of 0.8. Note that each vertical error bar in Figure 5 gives the error on the mean of all the points in that phase bin; the standard deviation of the points in each bin, which measures the spread of the data points around the mean, is larger (by definition) and plotted on the bottom axis. We emphasize this distinction because the small error bars in Figure 5 imply only that there was a well-defined *mean* pulse profile during the relevant pre-eclipse time interval, but do not rule out the possibility that significant amplitude fluctuations may also have occurred. Nevertheless, the combination of a highly sinusoidal mean pulse shape and the total absence of power at the first overtone frequency does allow us to discard models that predict more complex light modulations (see Section 4).

With the filtered data sets and good estimates of the pre-eclipse oscillation periods in hand, we proceeded to fit sinusoids of fixed period (28.77 s for Run 3; 28.60 s for Run 4) to blocks of data containing 16 points (3 oscillation cycles) each. Following NR74, we allowed approximately 50% overlap between successive data segments being fit. The results of demodulating both PRISM time series in this way are shown in Figure 6. In the top panels of this figure, we plot again the white-light light curves themselves, with insets showing small sections of the light curves complete with error bars. Note that the 29-s oscillations can actually be seen directly even in the unfiltered data. The lower panels show the filtered light curves, the oscillation amplitudes and the oscillation phases determined from the sinusoid fits. The filtered light curves and oscillation amplitudes are shown in both absolute (ergs cm^{-2} s^{-1} Å^{-1}) and relative (percentage of total light at that phase) units in order to test if and how the oscillation amplitudes are correlated with the total flux at a given orbital phase.

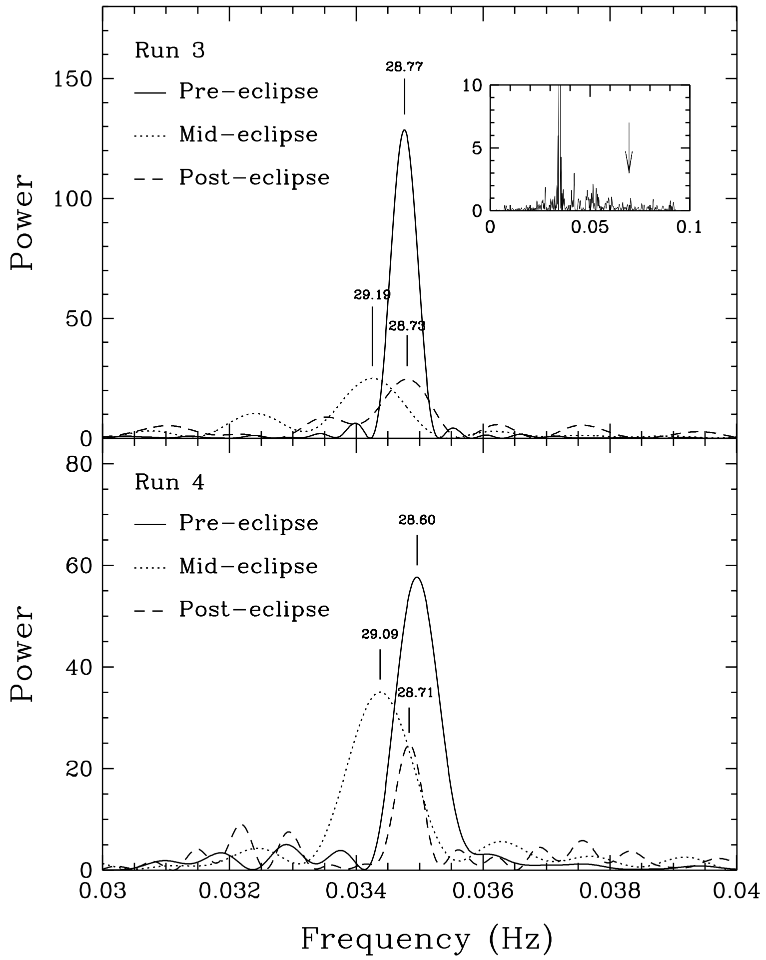

Fig. 4.— Lomb-Scargle power spectra for the pre-, mid- and post-eclipse segments of the high-pass filtered light curves of Run 3 (top panel) and Run 4 (bottom panel). The peak in each power spectrum is marked with the period (in seconds) to which it corresponds. The inset in the top panel shows the pre-eclipse power spectrum for Run 3 over a larger frequency and smaller power range. The arrow marks the position of the (absent) first overtone of the 28.77 s period in this part of the data.

Perhaps the most important new result from Figure 6 is that orbital phase-linked amplitude variations are clearly detected for the first time in UX UMa. The absolute amplitudes are greatest at pre-eclipse orbital phases, decline during eclipse and recover only slightly at post-eclipse phases. When expressed as a fraction of the total light at a given orbital phase, the oscillation amplitudes (which are about 0.5% at pre-eclipse phases) exhibit only a weak eclipse feature, but show some spikes just before and after eclipse. This indicates that the oscillation eclipse is similar in relative depth to that of the total light, but has a slightly narrower width.

Our detection of oscillation eclipses contrasts with the apparent absence of orbital phase-related amplitude modulations in the observations analyzed by NR74. Since their data were of much lower quality, it is not clear how much weight should be attached to this difference. NR74 estimate that amplitude changes greater than a factor of two would probably have been detectable in their data—a criterion satisfied by the eclipses of the oscillations in our observations. However, to combat noise, NR74 found it necessary to average over several eclipses in their search for amplitude modulations, so their non-detection might have been caused by secular and/or stochastic variability between runs. The amplitudes of the oscillations in our data certainly do exhibit sizeable fluctuations even away from eclipse. More high-quality data will be required to decide whether

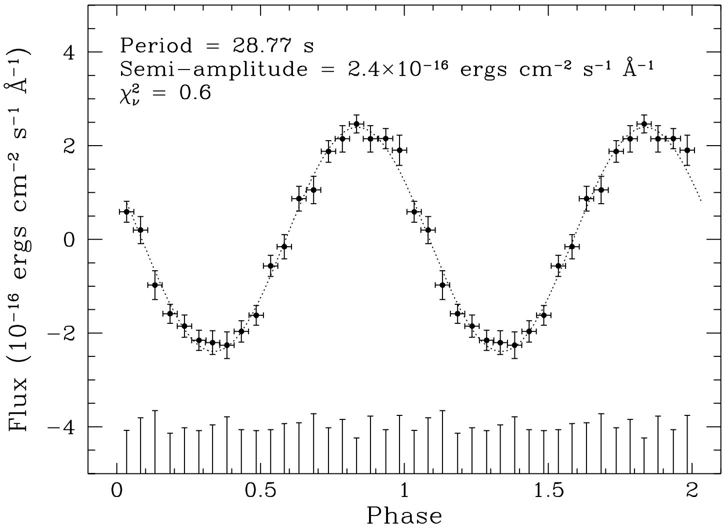

Fig. 5.— The result of folding the pre-eclipse, high-pass filtered white light time series derived from Run 3 onto the 28.77 s oscillation period. The data have been binned to a phase resolution of 0.05 (marked by the horizontal error bars) and are shown repeated over two oscillation cycles for clarity. The vertical error bars correspond to the error on the mean of the data points in each bin; the size of the vertical bars shown at the bottom axis corresponds to the standard deviation of the points in each bin around the mean value. The dotted line is the best-fitting fixed-period sinusoid for this data set. Based on its reduced χ^2 of 0.6, the fit describes the data acceptably.

UX UMa's 29-s oscillations always undergo eclipses or not.

The eclipse-related phase shift noted by NR74 is easily seen in Figure 6. The absolute value of the total shift over the course of the eclipse actually appears to be somewhat larger than 360° in our data. However, it is possible that the post-eclipse oscillations once again attained more accurate coherence with their pre-eclipse counterparts at orbital phases beyond the end of the PRISM observing sequences. For Run 3, at least, Figure 6 also hints at the phase shift progressing in three stages. First, there appears to be a relatively steep, approximately linear decline. Next, there is a short interval just after mid-eclipse in which there is essentially no further phase drift. Following this, the shift is completed in roughly the same manner as in the first stage. However, given the limited amount of data on which it is based, this description is probably not unique. NR74 also saw a departure from linearity in the phase shifts they detected, which they described as a BS-related "lump".

Since different periods were used in the sinusoid fits to the Run 3 and 4 data, the oscillation phases predicted by the fits cannot be compared between runs. In Figure 6, we have therefore shifted the oscillation phases derived from both runs to a common mean pre-eclipse value of 180°. It would nevertheless be useful to determine whether the oscillations in both runs could have been coherent with each other if the true (out-of-eclipse) oscillation period is assumed to have remained constant. In that case, the difference between the values measured from the relevant power spectra ($\Delta P = P_{Run\ 3} - P_{Run\ 4} = 0.17$ s) would have to be attributed to observational error. Adopting $P = 28.7$ s as an estimate of the oscillation period and noting that the time difference between the end of Run 3 and the start of Run 4 is approximately $\Delta t \simeq 47,000$ s, we find that the uncertainty in the cycle count would be about $\Delta E = (\Delta t \Delta P)/(P^2) \simeq 10$ cycles at the start of Run 4. Thus the data cannot be used to test the coherence properties of the oscillations on time scales as long as the gap between Runs 3 and 4 (about 2.8 orbital periods).[3]

We have also tried to establish more securely whether the 29-s oscillations were present during

[3]One might alternatively estimate P and ΔP (and hence ΔE) from the number of cycles contained in a given run and the time resolution of the observations. However, with this method we still predict $\Delta E \simeq 2.8$ cycles, even under the optimistic assumption that an entire run could be used as the baseline in the required cycle counts.

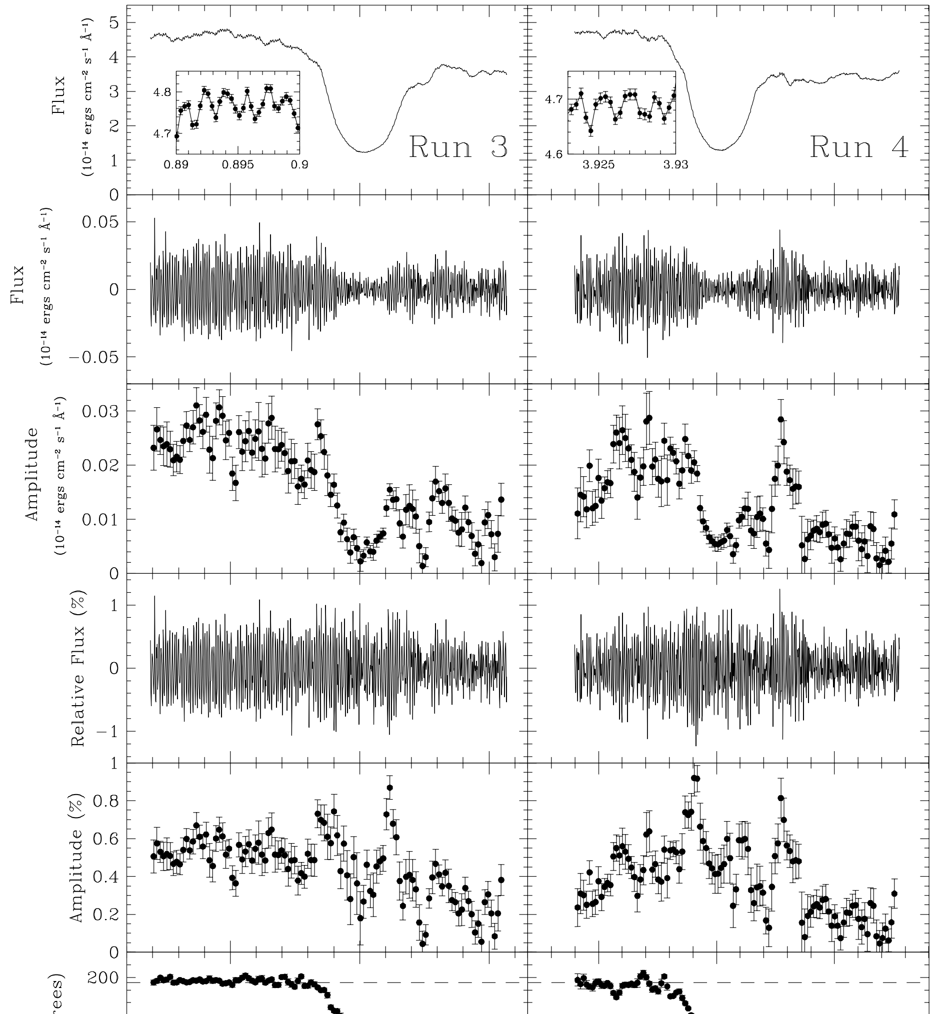

Fig. 6.— The results of high-pass filtering and demodulating the white light (2000 Å–8000 Å) light curves for Runs 3 (left panels) and 4 (right panels). From top to bottom, we show as a function of orbital phase: the unfiltered light curves (insets zoom in on small portions of the data), the high-pass filtered light curves, the oscillation amplitudes derived from the latter, the high-pass filtered light curves expressed as a percentage of the total light at a given phase, the oscillation amplitudes derived from the latter and the phase of the oscillations. The oscillation phases for both runs have been shifted to a mean value of 180° at pre-eclipse orbital phases (see text). Only every other data points in the amplitude and phase plots is independent.

the August (G160L) observing sequences (Runs 1 and 2) despite the absence of any corresponding features in their power spectra in Figure 1. To this end, we first high-pass filtered the first order white-light light curves for these runs in a fashion identical to that used for the November (PRISM) time series. At phases away from eclipse, the filtered first order light curves showed fluctuations of $\sim 1.5\%$, which is consistent with the noise level in the unfiltered time series. We nevertheless proceeded to compute power spectra for the filtered G160L light curves, since sufficiently coherent periodic signals can sometimes be detected even if the signal-to-noise ratio is < 1 (Scargle 1982). However, no significant peaks corresponding to a 29 s period were found in these power spectra. By injecting artificial signals into the unfiltered time series, and analyzing the resulting fake data in the same way as the actual observations, we determined that we could have marginally (easily) detected a coherent sinusoidal modulation with amplitude 0.5% (1%) at this frequency.

As a final check, we also filtered and analyzed the zeroth order light curves in the same fashion. A (weak) signal near the expected period was seen only in the time series corresponding to the Run 2 post-eclipse data segment. Injecting artificial signals of known strength into this data set, we found that the corresponding oscillation amplitude was approximately 0.2%. This is less than the upper limit we are able to place on the oscillations in the UV first order light curves, but comparable to the amplitude of the oscillations around 3400 Å in the post-eclipse data segments of the PRISM observations. (The latter statement is based on the oscillation spectra presented in Section 3.2.) Given that this is the *only* data segment in the G160L observations in which UX UMa's 29-s oscillations may have been detected, we nevertheless conclude that for most of the time covered by the August observing runs, the oscillations must have been absent or weak compared to the November sequences. This difference between the August and November observations may be related to the fact that the system brightened by approximately 50% between the two epochs (see Section 4. That DNO periods and amplitudes are quite sensitive to changes in a system's brightness (and hence presumably the mass transfer rate) is known from observations of DNe on the rise or decline of an outburst (e.g., Patterson 1981; Hildebrand et al. 1980).

Finally, we note that some of the G160L power spectra did show a consistent and (in at least one case) significant power excess at somewhat shorter periods around 20 s. Judging from the size of the power peaks, the amplitude of the corresponding oscillations was probably just over 0.5% but well below 1%. Could these 20-s oscillations in the August data be the counterpart of the 29-s oscillations observed in November? This is certainly a tempting identification, especially since WN72 and NR74 both established that the period of the oscillations is not always the same. However, the shortest period ever detected for the 29-s oscillations is 28.5 s (NR74), significantly longer than the periods that are present in the G160L data sets. Selection effects could be responsible for this, and thus we cannot rule out that the two types of oscillations do share a common origin. However, the current observational database certainly does not yet establish any such link. Because of their relative weakness, we will not consider these 20-s oscillations further below.

3.2. *The Spectrum of the 29-s Oscillations*

To isolate the spectra of the 29-s oscillations, we first subtracted a 5-point (about 1 oscillation cycle) running mean from each wavelength pixel at each orbital phase separately for pre- ($\phi < 0.95$), mid- ($0.98 < \phi < 1.02$) and post-eclipse ($\phi > 1.05$) time intervals. The resulting flux difference was then added to either a positive or negative oscillation spectrum, depending on the sign of the flux datum at the same orbital phase in the similarly high-pass filtered white light light curve. After dividing the co-added positive and negative oscillation spectra by the number of orbital phase points used in their construction, the negative mean oscillation spectra were subtracted from the positive ones to yield the net oscillation spectra. Since the mean pulse shape is highly sinusoidal, the oscillation spectra were finally normalized to the peak-to-peak oscillation amplitude by multiplying the monochromatic fluxes by a factor of $\pi/2$ (the mean value of the positive/negative part of a sinusoidal pulse with zero mean and unit amplitude is $\pm 2/\pi$).

To characterize the oscillation spectra, we carried out χ^2 fits to the data using three different types of models: (1) a single temperature blackbody (BB); (2) a single temperature model stellar atmosphere (SA); (3) the derivative of the BB spectrum with respect to temperature, dB/dT. The SA models were calculated with Hubeny's spectral synthesis code SYNSPEC (Hubeny, Lanz, & Jeffery 1994) from ATLAS (for $T_{eff} \leq 50,000\ K$) or TLUSTY (Hubeny 1988; Hubeny & Lanz 1995) (for 50,000 K $< T_{eff} \leq 140,000$ K) structure models. The overall range of gravities on our model grid was $2.0 < \log\ g\ < 7.0$, though not all gravities were available at all temperatures. In the actual fits to the data, we found that models with the highest available gravity at a given temperature tended to be preferred (but note that model spectra tend to be more sensitive to temperature than to gravity in the relevant parameters regime). All model spectra were smoothed to the instrumental resolution before comparing them to the data, and E(B–V)=0.0 was assumed in all fits (c.f., Paper I).

Models (1) and (2) are appropriate if the observed oscillations have their origin in a more or less constant temperature emitting region whose projected area, as seen from Earth, is varying in a periodic fashion. Model (3) would be preferred if the oscillations are due to a source presenting us with roughly constant projected area (away from eclipses, at least), but fluctuating in temperature. Note that while the normalization constant required to match models (1) and (2) to the data is simply proportional to the ratio of projected area and distance squared, the same normalizing factor for model (3) includes an additional multiplicative term which is equal to the magnitude of the temperature fluctuations, ΔT. Thus while models (1) and (2) can be used straightforwardly to place constraints on the size of the emitting region, the same is not true of model (3).

The pre-, mid- and post-eclipse oscillation spectra constructed from the Run 3 and 4 observing sequences are plotted along with the best-fitting models in Figures 7 and 8. The parameters/limits derived from the model fits to the oscillation spectra are listed in Table 5. The spectrum of the oscillations is extremely blue at orbital phases away from eclipse. The model fits to these data all converge on effectively infinite temperatures, suggesting that we may be seeing the Rayleigh-Jeans tail of the oscillation spectrum. [Note that the dB/dT model also has Rayleigh-Jeans-like tail: in the limit $(h\nu)/(kT) \rightarrow 0$, $dB/dT \propto B(T)/T$ asymptotically, where all symbols have their usual meanings.] Our model fits nevertheless allow us to derive lower limits on the temperature of the source of the oscillations at these phases. Inspection of Table 5 shows that $T > 130,000$ K, 100,000 K and 50,000 K at the 2σ level for all BB, SA and dB/dT models, respectively. For the BB and SA models, the lower limits on the temperature of the source can be directly transformed into upper limits on its projected area, A_{proj}. These turn out to be $A_{proj}/A_{WD} < 0.01$ and 0.02 for all BB and SA models, respectively, where $A_{WD} = 4\pi R_{WD}^2$ is the surface area of the WD and a distance of 345 pc to UX UMa has been assumed (Baptista et al. 1995). We conclude that if our optically thick, thermal models are appropriate, the oscillation light away from eclipse is dominated by a very compact and extremely hot source.

The insets in the top panels of Figures 7 and 8 show the ratio of the pre-eclipse oscillation spectra to the total average pre-eclipse spectra (c.f. Paper I) as a function of wavelength. These plots demonstrate explicitly that the colors of the oscillations are much bluer than those of the disk and the bright spot. Specifically, the peak-to-peak amplitude of the oscillations at pre-eclipse orbital phases rises from well under 1% of the total light at long optical wavelengths to $\gtrsim 2\%$ near 2000 Å. This wavelength dependence may be the reason why the amplitude of the oscillations in our white-light PRISM light curves ($\simeq$ 0.5%) is somewhat larger than in the ground-based optical observations of WN72 and NR74, since the latter were not sensitive to the shortest wavelengths covered by the PRISM. As a simple test of this idea, we have estimated the mean strength of the oscillations in the wavelength region 3000 Å–8000 Å from the Run 3 pre-eclipse data segment (in which the oscillations are strongest). The expected amplitude of the oscillations in that bandpass is about 0.25%, close to that found by WN72 and NR74.

The mid-eclipse oscillation spectra in Figures 7 and 8 are rather noisy, but nevertheless markedly redder than the pre- and post-eclipse oscillation spectra. Correspondingly, model fits to these data yield much cooler temperatures in the range 20,000 $K \lesssim T \lesssim 30,000$ K (BB and SA models) or 10,000 $K \lesssim T \lesssim 20,000$ K (dB/dT model). The projected areas corresponding to the BB and SA model fits are of the order of a few (2–7) percent of the WD surface area. Note that all of our estimates are subject to revision if the pulsed emission is optically thin or is due to reflection of light from a hidden source (see below). In particular, the emitting region could then be much larger than suggested by the BB and SA model fits. In any event, what remains of the oscillation light at mid-eclipse appears to be coming from a region that is cooler and more extended than the source which dominates the oscillations at orbital phases away from eclipse.

4. DISCUSSION—THE ORIGIN OF THE 29-s OSCILLATIONS

The properties of UX UMa's 29-s oscillations place fairly stringent constraints on models for their origin. This is important in its own right, but assumes a more general significance because, as noted in the Section 1, DNOs are observed in a fair

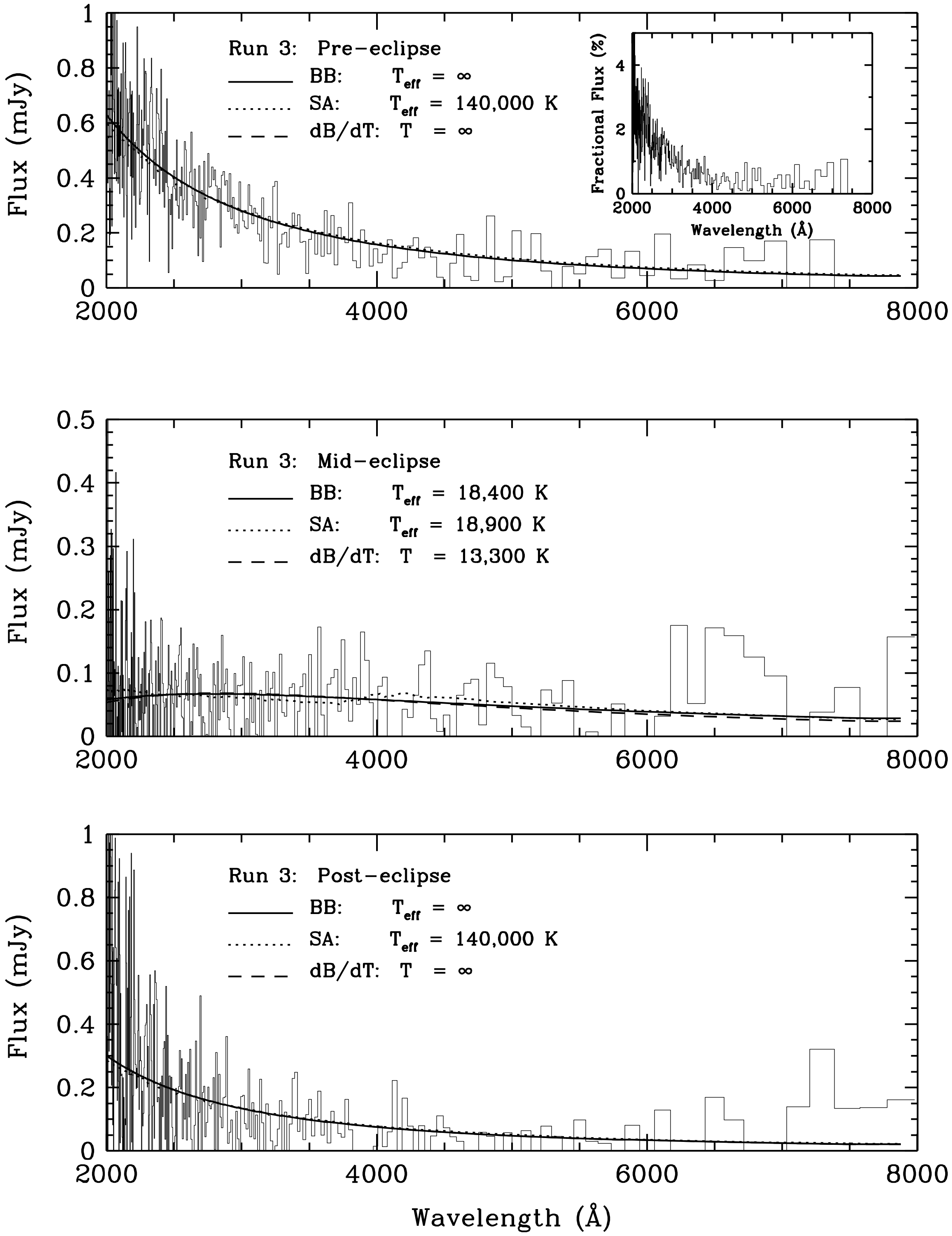

Fig. 7.— The pre- (top panel), mid- (middle panel) and post-eclipse (bottom panel) spectra of the 29-s oscillations during Run 3 are shown as the thin histograms. The best-fitting BB, SA and dB/dT models are also shown. The inset in the top panel shows the same oscillation spectrum with the flux expressed as a percentage of the flux at a given wavelength in the overall pre-eclipse spectrum.

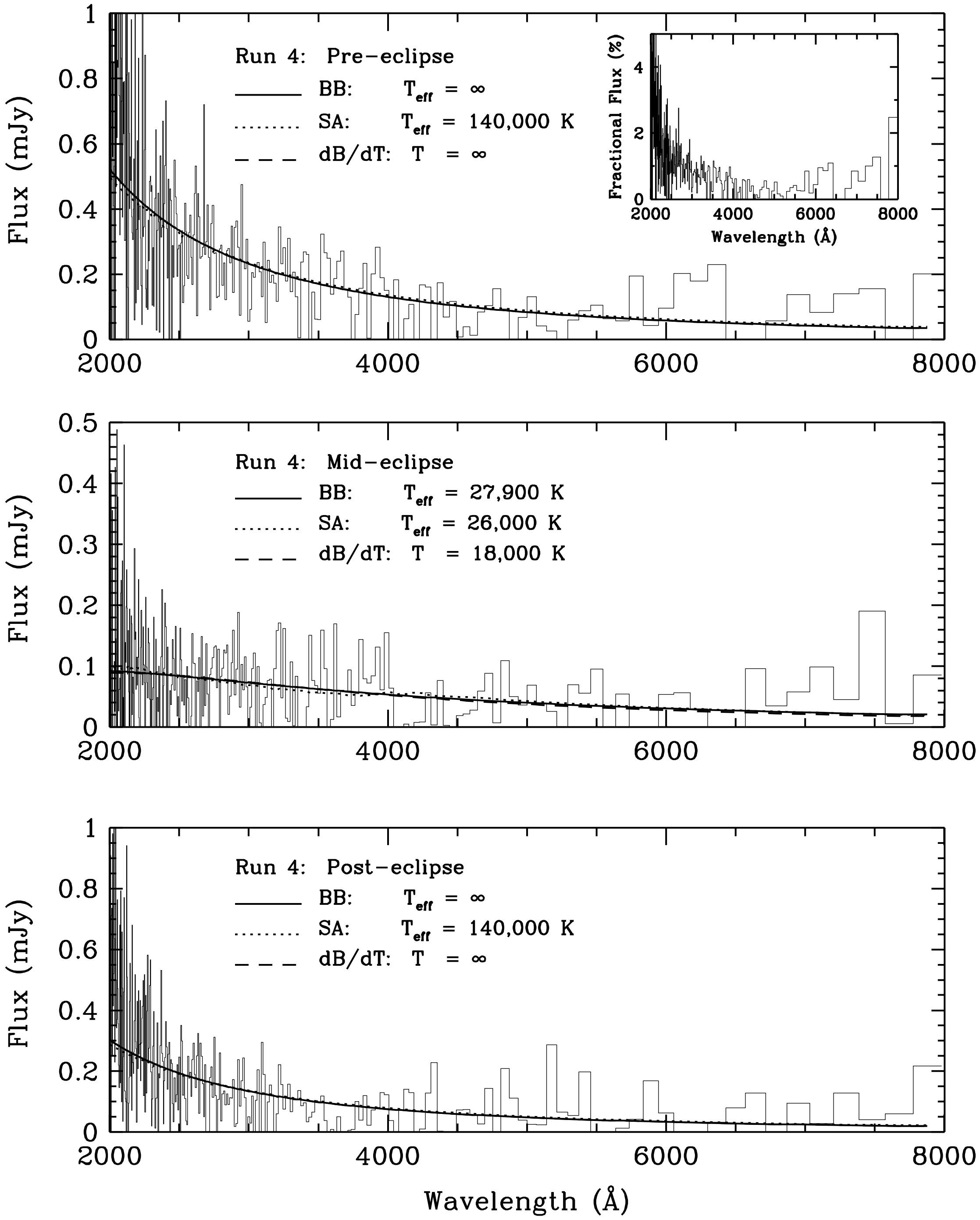

Fig. 8.— As Figure 7, but for the Run 4 data.

number of DNe and a few other NLs (e.g., Warner 1995).

Most fundamentally, it seems likely that the short time-scale of the oscillations corresponds to the dynamical (rotational) time-scale near the source of the oscillations. For UX UMa's system parameters ($R_{WD} = 0.014 R_{\odot}$, $M_{WD} = 0.47 M_{\odot}$; Baptista et al. 1995), 29 s corresponds to the Keplerian rotation period at a radius of about 1.1 R_{WD} in the accretion disk, i.e., very close to the WD. The very blue spectrum of the oscillations away from eclipse similarly suggests that their main source is very compact and extremely hot. These constraints are consistent with an origin of the oscillations either in a small hot spot on a fast rotating WD, or in a BL between the inner edge of the disk and the WD, but they would seem to pose serious problems for any model in which the source of the oscillations is identified with a disturbance further out in the accretion disk. On the other hand, the shapes of the oscillation eclipses—specifically their non-totality and gradual in- and egresses—demand that not all of the emission can come from near the center of the disk. This is because these regions, including the entire WD, are completely and rather abruptly occulted by the secondary near mid-eclipse.

We are thus already forced to consider a two component model for the origin of the observed modulations. The first of these components dominates the light at orbital phases away from eclipse and is probably due to a compact emitting source near disk center. This source is fully eclipsed by the secondary near conjunction. The second component is probably due to reprocessing of the light emitted by the compact source in the accretion disk atmosphere, and is not fully occulted even at mid-eclipse. The suppression of the oscillation amplitudes at post-eclipse orbital phases also seems to implicate the bright spot region at the disk edge as a possible reprocessing site. However, this interpretation is not unique, since some kind of post-eclipse absorption event could also produce the observed asymmetries in the light curves of both the oscillations and the total light. The same interpretive difficulty was noted in a different context in Paper I.

Note that we use the term "reprocessing" loosely here, in the sense that the corresponding spectral component could in principle be due to either thermalization or reflection of the pulsed light emitted by the compact source. It might also represent recombination radiation emitted in response to photoionization of material in the disk atmosphere by the hot, compact source.

A two component model such as that sketched above is also required to account for the difference between the oscillations spectra away from and during eclipse. The former are very blue and appear to be produced by a compact, hot source. By contrast, the latter are much redder and seem to arise in a cooler and more extended region. Note, however, that the area estimates provided by our BB and SA model fits to the mid-eclipse oscillation spectra, while larger than the corresponding estimates for the out-of-eclipse spectra, are still only a few percent of the WD surface area. This is much smaller than the portion of the accretion disk that is visible at mid-eclipse. (Based on UX UMa's system parameters, we estimate that more than half of the disk surface area remains unocculted at all times.) It should be kept in mind, however, that the models we have used to fit and characterize the data are optically thick, whereas at least the reprocessing component revealed in the mid-eclipse oscillation spectra might not be. If this component is in fact optically thin, the reprocessing site could be much larger than suggested by our fits. We can also not exclude the possibility that the hot, "compact" component we observe could itself be due to reflection. In this case the "true" source of the oscillations must be hidden from view and could also be larger than indicated by our model fits to the out-of-eclipse spectra.

A related potential problem faced by this type of model is the apparent dichotomy between the very blue out-of-eclipse oscillation spectrum—which might be taken to indicate that the compact, hot component dominates almost completely at these orbital phases—and the rather gradual eclipses of the oscillations in Figure 6—which suggest that a relatively large area contributes significantly to the oscillations away from eclipse. However, we have not yet tried to fit any two component models to the out-of-eclipse oscillation spectra. (This is partly because the χ^2 values produced by our single component model fits to these relatively noisy data were already low, and partly because such an analysis lies beyond the scope of the present paper.) Consequently, we are unable to set a limit on the possible contribution of the extended, reprocessing component to the oscillating flux away from eclipse. In the absence of such a constraint, we cannot tell if there might be a conflict between the data and a simple two component model.

A qualitative constraint on the relative strength of the two components may be derived from the fact that the oscillations lose one cycle during eclipse. Quite generally, if the 29-s oscillations are associated with prograde rotation of the emitting source(s), a significant and probably dominant fraction of the emission must be beamed in such a way as to produce pulse maxima when the corresponding emitter is nearest to us. Only then will successive pulse maxima occur later and later after the limb of the secondary first passes over the line of centers of the two stars in the system. An obvious example of an emitting source meeting this constraint would be a bright spot on the surface of a fast rotating WD (Petterson 1980). By contrast, if the oscillations were dominated by the reprocessing of light emitted by such a spot in the atmosphere of a concave, optically thick accretion disk, pulse maxima would be expected to occur when the spot is illuminating the far side of the disk, which is less obliquely inclined towards our line of sight. In that case, the oscillations would gain a cycle during every eclipse, a situation that is actually encountered in the IP DQ Her (e.g., Zhang et al. 1995). Thus with a two component model including a directly observed and a reprocessed component, both positive and negative eclipse phase shifts can be accounted for. In the general scenario, in which both the compact source of direct light and the extended reprocessing disk contribute significantly to the modulated flux, the sign of the observed phase shift will depend on the relative strength of these two components (Petterson 1980). The negative phase shift in UX UMa thus suggests that the direct, compact component contributes the majority of the oscillation light away from eclipse, provided that the optically thick accretion disk is the main reprocessing site.

A final constraint on the origin of the oscillations can be derived from the observed pulse shape away from eclipse (Figure 5). Let us assume for the moment that the oscillations at these orbital phases are dominated by direct light from a rotating, compact source which presents us with varying amounts of projected area over the course of an oscillation cycle. More specifically, we will identify this compact source with either a bright spot on the surface of a fast rotating WD or with a localized disturbance in an equatorial BL at the inner disk edge. Now the highly sinusoidal pulse shape implies that this compact source is never fully occulted during the oscillation cycle. This rules out any site for the compact source lying within $\lesssim 3\ R_{WD}$ of disk center in the equatorial plane, since all locations closer in will be occulted once during every cycle by the body of the WD. Thus the identification of the compact source with a disturbance in the inner disk or an equatorial BL is problematic. Similarly, Petterson's (1980) numerical model for the 29-s oscillations—which is essentially identical to our two component (direct + reprocessed) model, but explicitly relies on bright spots on the equator of the rotating WD—is ruled out by the new data since it predicts a non-sinusoidal pulse shape.

Can magnetically controlled accretion near the WD provide a more promising alternative? In the simplest version of this picture, the magnetic field of the WD is strong enough to disrupt the inner disk and force the accreting material to flow along field lines onto one or both magnetic polecaps. The impact of the accretion flow onto the poles produces one or two bright spots on the WD surface which can then be identified with the compact source that dominates the observed 29-s oscillations away from eclipse. This model is essentially just a weak field IP scenario for UX UMa.

If both accreting poles were visible to us, the period of the oscillations would correspond to one half of the spin period of the WD or, equivalently, to one half of the rotation period of material near the inner disk edge. However, this would imply an inner disk radius of 1.8 R_{WD}, whereas a hole extending out to 3.1 R_{WD} would be required for the second pole to be unocculted by the optically thick inner disk. Thus only one of the magnetic poles can actually be visible in UX UMa. It is nevertheless easy to explain the sinusoidal pulse shape within an IP framework, since it is only required that the inclination of the magnetic axis with respect to the disk and WD rotation axes be small enough for the visible accreting pole to avoid self-eclipses. For UX UMa's orbital inclination of $i = 71^o$ (Baptista et al. 1995), the maximum allowed inclination of the magnetic axis is $90^o – i = 19^o$.

In an IP model with a single visible pole, we can identify the oscillation period directly with the WD spin period and the Keplerian period near the inner disk edge. Thus the accretion disk must extend down to about 1.1 R_{WD} before magnetic stresses disrupt it.[4] This may be identified with the radius of the WD magnetosphere (the Alfvén radius), which for a disk threaded by a dipolar field is located at roughly (Frank, King, & Raine 1985)

$$R_A \simeq 2.5 \times 10^8 \dot{M}_{16}^{-2/7} M_{WD}^{-1/7} \mu_{30}^{4/7} cm \qquad (1)$$

where the parameters have been scaled to units appropriate for CVs, i.e., M_{WD} is the mass of the

[4]Note that if the the period of the oscillations corresponded to the spin period of the WD, but the inner edge of the disk were located much farther out than 1.1 R_{WD}, material at the inner disk edge would be rotating more slowly than the field lines it is trying to latch onto. It would therefore be repelled out to larger radii and perhaps even out of the system by this centrifugal barrier. This propeller mechanism is thought to operate in the intermediate polar AE Aqr (Eracleous & Horne 1996).

accreting WD in solar masses, $\dot{M}_{16}$ is the accretion rate in units of 10^{16} g s^{-1} and μ_{30} is the magnetic moment of the WD in units of 10^{30} G cm^3. Taking UX UMa's system parameters, $\dot{M}_{16} \simeq 10-100$, and setting $R_A = 1.1R_{WD}$, we find $\mu_{30} \simeq$ 30–100, at the low end of the range for IPs, as it must be (Warner 1995).

However, there are two objections to the direct application of an IP model to UX UMa. The first is that it requires the WD to be rotating at more than 90% of break-up, which might be considered to be a uncomfortably high value. On its own, this objection could actually be turned around to provide an explanation for the "missing BL" problem in "non-magnetic" CVs (see Hoare & Drew 1991; Hoare & Drew 1993 and references therein).[5]

The second objection is more potent and arises from the changes in the oscillation period that were observed by NR74. For example, during one of their multi-night observing sequences, the period changed roughly monotonically from 30.0 s to 28.5 s within the course of only 5 days. This corresponds to a period derivative $\dot{P} \sim -3 \times 10^{-6}$ s s^{-1} and a time-scale for period changes of $\tau_{spin-up} = P/(-\dot{P}) \simeq 8 \times 10^6$ s ~ 100 days. This should be compared to the minimum spin-up time-scale that can be achieved by any type of accretion (magnetic or otherwise). This minimum time-scale is obtained by considering the time required to spin-up the WD from rest to break-up if *all* of the angular momentum of the accreting matter goes into WD rotation. A simple calculation gives

$$\tau_{spin-up} \sim \frac{M_{WD}}{\dot{M}_{acc}} \left(\frac{R_{WD}}{R_{circ}}\right)^{1/2} \quad (2)$$

where R_{circ} is the circularization radius of of the accreting material. For UX UMa's system parameters, $R_{circ} \simeq 12.5R_{WD}$ and $\tau_{spin-up} \sim 10^7$ years for reasonable accretion rates between $10^{17} - 10^{18}$ g s^{-1}. This tremendous discrepancy with the time-scale over which the oscillation period is seen to vary shows that the observed period changes in UX UMa cannot possibly reflect actual WD spin period variations in response to accretion. Thus the simple IP model for UX UMa fails.

Warner (1995) has recently proposed a qualitative unified scheme for DNOs, which may offer a way out of this dilemma. Building on a model described originally by Paczyński (1978) (see also King 1985), he suggested that DNOs occur as a result of magnetic accretion in systems in which the WD magnetic field is weak enough to permit the outer layers of the WD to rotate differentially. In this case, the observed DNO periods correspond not to the spin period of the entire WD, but to the rotation period of its surface layers. The observed spin-up time scales can then be explained, since M_{WD} in Equation 2 can now be replaced by the mass of the rotating layers only (which must be $\lesssim 10^{-8} M_{\odot}$). Thus, changes in the oscillation periods can plausibly be accounted for by accretion rate variations in this model. Since magnetic accretion will only occur at all if $R_A > R_{WD}$, DNOs should not be present in all "non-magnetic" CVs, as is observed. Moreover, relatively more DNe than NLs should exhibit DNOs, since the latter will on average have higher mean accretion rates and smaller magnetospheres. This, too, is in line with the available data.

What about the apparent absence of the oscillations during the August observations, when the system was 50% fainter than in November? A qualitative explanation for this behaviour is suggested by outburst observations of the dwarf nova AH Her (Hildebrand et al. 1980). In this system, DNOs are present on the rising and declining outburst branches, with amplitudes (periods) that increase (decrease) with increasing brightness. However, near maximum light at the peak of the outburst, the DNOs suddenly disappear. In the context of a magnetic accretion model, this suggests that the magnetosphere shrinks in response to an increase in the accretion rate just as expected. The growth of the DNO amplitudes occurs because more accretion energy becomes available for generating the oscillations as the disk-magnetosphere interaction region moves towards smaller radii. The DNO periods decrease because the Keplerian velocities increase towards disk center. These trends continue until the magnetosphere is crushed onto the WD surface, at which point the DNOs cease abruptly. Thus an increase in DNO amplitude with increasing accretion rate, as suggested by UX UMa, need not be in conflict with a magnetic accretion model.

Despite this apparent success, we feel it is too early to accept a model of this type for the origin of DNOs. Most importantly, we are not sure what magnetic accretion onto differentially rotating WD surface layers really means physically. For example, it is not clear *a priori* whether the magnetic field controlling the accretion flow should be thought

[5] In a magnetic accretion scenario there would of course be no classical BL anyway, but unless the WD is a rapid rotator, roughly one half of the accretion luminosity would still have to be released from a very small region at the center of the accretion disk. Thus the "missing BL" problem would simply become a "missing flux" problem in this case, which is probably a more appropriate view in any case.

of as stable and anchored in the slowly rotating WD core or, alternatively, as transient and perhaps generated, as well as anchored, in the differentially rotating surface layers themselves (possibly by some sort of dynamo action; e.g., King 1985). Partly as a result of this uncertainty, it is also not obvious what type of accretion geometry should be expected in this picture close to the WD surface. Thus more theoretical work will be required before a magnetic accretion scenario of this kind may be judged successful.

As an incentive for theoreticians to tackle this problem, we conclude this section by placing UX UMa's 29-s oscillations in the context of DNOs more generally. Combining data from Warner (1995) and Ritter (1990), we plot in the bottom left panel of Figure 9 DNO period against WD mass for all systems in which DNOs are observed and for which WD masses are available. Each continuous curve in Figure 9 gives the Keplerian rotation periods in an accretion disks around a primary of the given mass at the indicated radius in the disk. The analytical approximation of Nauenberg (1972) to the Hamada & Salpeter (1961) mass-radius relationship for cool degenerate stars has been assumed in deriving these curves. Where vertical error bars are shown, they correspond to the range of periods that have been observed in the system.

Several points are worth noting from this plot. First, the periods of all DNOs correspond to the Keplerian time-scales at radii $R_{DNO} \simeq 1 - 3\ R_{WD}$ in the accretion disk. In no case are the DNO periods inconsistent with the basic requirement that $R_{DNO} > R_{WD}$. Second, several DNe exhibit period variations similar to or larger than those noted above for UX UMa. Thus the identification of DNO periods with WD spin periods is untenable in these systems also. Third, the two IPs that might be said to exhibit DNOs (AE Aqr with $P_{DNO} = 33$ s and DQ Her with $P_{DNO} = 71$ s) both occupy the region close to the $R_{DNO} = 3\ R_{WD}$ line in Figure 9. This would appear to be consistent with a magnetic accretion scenario since the field strength (and hence magnetospheres) should be larger in these systems than in DNe and NLs. However, in both of these systems the oscillation periods are extremely stable and almost certainly do correspond to the true WD spin period (or perhaps one half of it, in the case of DQ Her; Zhang et al. 1995). Fourth and finally, there may be a hint of clustering near $P_{DNO} \simeq 30$ s in Figure 9.

This last property is seen more easily in a simple histogram of the observational DNO-period distribution function which we show in the bottom right panel of Figure 9. The cluster of CVs with $P_{DNO} \simeq 30$ s is fairly obvious in this figure. For comparison, the WD mass distribution function for these systems is plotted in the top left panel of Figure 9. This histogram does not seem to show a similarly sharp peak, but the relatively large errors on the WD mass estimates may be partly responsible for this. (A clustering of oscillation periods could be easily explained by any model in which P_{DNO} is set by the dynamical time-scale near the WD *if* the WD mass distribution function showed a similar peak.) In any case, the currently known number of CVs that exhibit DNOs and have sufficiently well established periods is probably too small for the peak in the DNO-period function to attain statistical significance. However, if the clustering of oscillation periods around 30 s is confirmed in the future and shown *not* to arise simply from the underlying WD mass distribution function, this property will have to be accounted for by any successful model for the origin of DNOs.

5. CONCLUSIONS

Low amplitude ($\simeq 0.5\%$) coherent 29-s oscillations have been detected in HST/FOS eclipse observations of the NL variable UX UMa. These are the same DN-type oscillations that were originally discovered in this system by WN72 and subsequently analyzed in more detail by NR74. The oscillations are easily seen in one pair of eclipse sequences obtained with the FOS/PRISM in November of 1994, but not in a similar pair obtained with the FOS/G160L grating in August of the same year (except, perhaps, in one isolated data segment of the zeroth order light curves; see Section 3.1).

We find that the oscillations in the PRISM data are sinusoidal to within the small observational errors and undergo an approximately -360° phase shift during eclipses (i.e., one cycle is lost). These results are similar to those derived by WN72 and NR74. We also detect orbital phase-related amplitude variations in the oscillation time series. Specifically, the oscillation amplitudes are highest at pre-eclipse orbital phases and exhibit a rather gradual eclipse whose shape is roughly similar to, though perhaps slightly narrower than UX UMa's overall light curve in the PRISM bandpass (2000 Å–8000 Å).

PRISM spectra of the oscillations constructed from data segments covering pre- and post-eclipse orbital phases are extremely blue. Single component, optically thick model fits to these data only allow limits to be placed on the source temperature and size. In fits to the data with BB (SA) models, the lower limits on temperature always turn out to be

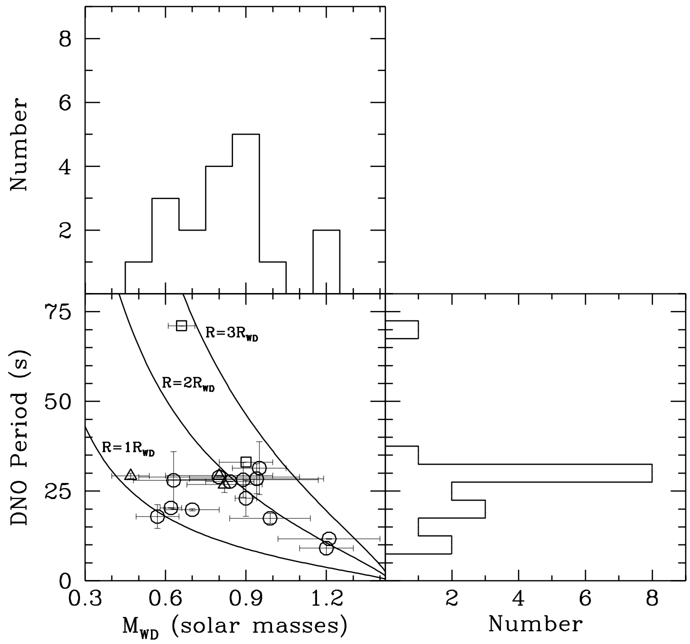

Fig. 9.— *Bottom left:* The oscillation period versus WD mass relation for all CVs with mass determinations that are known to exhibit DN-type coherent oscillations. Open circles are DNe, open triangles are NLs, open squares are DQ Her systems (DQ Her and AE Aqr). Vertical error bars correspond to the range of oscillation periods that have been seen in each system. Oscillation periods and ranges have been taken from Warner (1995); white dwarf masses and errors have been taken from Ritter (1990), except for UX UMa for which the mass estimate of Baptista et al. (1995)—$M_{WD} = 0.47 \pm 0.07 M_{\odot}$—has been used. The continuous solid lines mark the rotation periods at the indicated radii in a Keplerian accretion disk around a WD of given mass. *Bottom right:* Histogram of the DNO period distribution function. This is just the projection of the data in the bottom left panel onto the y-axis. *Top left:* Histogram of the WD mass period distribution function. This is just the projection of the data in the bottom left panel onto the x-axis.

$\geq 95,000$ K ($\geq 85,000$ K), and the corresponding upper limits on the projected area of the source are all $\leq 2\%$ of the WD surface area. Fits to the same data with the derivative of the blackbody spectrum, dB/dT—which would be appropriate if the observed oscillations were due to a source fluctuating in temperature (rather than to a source fluctuating in projected area)—also tend to converge towards infinite temperatures and yield lower limits $\geq$ 50,000 K. Thus the spectra and model fits all suggest that the source dominating the oscillations away from eclipse is extremely hot and probably very compact.

By contrast, the two oscillation spectra derived from data segments covering mid-eclipse are much redder. Correspondingly, model fits to these data yield cooler temperature estimates in the range $20,000 \text{ K} \lesssim T \lesssim 30,000$ K (BB and SA models) and $10,000 \text{ K} \lesssim T \lesssim 20,000$ K (dB/dT model). The projected areas corresponding to the BB and SA model fits to the mid-eclipse oscillation spectra are of the order of a few percent of the WD surface area. Thus what remains of the oscillation light at mid-eclipse appears to be coming from a region that is cooler and more extended than the source which dominates the spectrum of the oscillations at orbital phases away from eclipse.

Based on these observational constraints, we suggest that the ultimate source of the oscillations is probably a hot, compact region near disk center, although significant reprocessing of the light emitted by this source in the accretion disk and probably the BS must also take place. This kind of two component (direct + reprocessed) model appears to be able to account for all of the observed behavior, although it remains to be seen whether the very blue oscillation spectra away from eclipse can be reconciled quantitatively with the relatively broad and gradual eclipses of the oscillations in this picture. It should also be noted in this context that if the reprocessed emission is optically thin, the reprocessing site may be much larger than suggested by our optically thick model fits to the mid-eclipse oscillation spectra.

One *a priori* possible identification of the hot, compact source in this model is with a disturbance in the inner disk ar a classical, equatorial BL. However, the highly sinusoidal pulse shape of the oscillations does not permit this. The compact source might instead be identified with a bright spot on the surface of the rotating WD that, in an IP-type model for the origin of the oscillations, may be associated with an accreting magnetic pole. However, a standard weak-field IP model for UX UMa can also be ruled out, since WN72 and NR74 observed the oscillation period to change on time-scales much shorter than the minimum time-scale required to spin-up the WD by accretion torques. A scenario along the lines recently proposed by Warner (1995), in which the oscillations arise as a result of magnetic accretion onto differentially rotating WD surface layers, is still viable, but requires more theoretical work before it may be judged successful.

We finally note that the characteristics of UX UMa's oscillations place them quite squarely among DNOs in other CVs. In all systems, the period of the oscillations corresponds to the dynamical time-scale in the accretion disk at $1 - 3R_{WD}$. There is a hint that DNO periods may cluster around $P_{DNO} \simeq 30$ s despite the absence of a corresponding peak in the WD mass distribution function. However, since the number of CVs with established DNO periods and known WD masses is quite small, whereas errors on WD masses are relatively large, the reality and significance of this clustering needs to be confirmed.

Acknowledgements

We gratefully acknowledge the support of NASA through HST grant GO-5448 without which this work would not have been possible. In addition, RAW acknowledges financial support from NASA through grants NAGW-3171 and from ST ScI through grant GO-3683.03-91A, both to the Pennsylvania State University. We would also like to thank Chris Mauche, Ivan Hubeny and Rene Rutten for their contributions to this project, and the anonymous referee for a very helpful report.

REFERENCES

Baptista, R., Horne, K., Hilditch, R. W., Mason, K. O., & Drew, J. E. 1995, ApJ, 448, 395

Eracleous, M., & Horne, K. 1996, ApJ, 471, 427

Frank, J., King, A. R., & Raine, D. J., Accretion Power in Astrophysics (Cambridge: Cambridge University Press)

Hamada, T., & Salpeter, E. E. 1961, ApJ, 134, 683

Hildebrand, R. H., Spillar, E. J., Middleditch, J., Patterson, J., & Stiening, R. F. 1980, ApJ, 238, L145

Hoare, M. G., & Drew, J. E. 1991, MNRAS, 249, 452

Hoare, M. G., & Drew, J. E. 1993, MNRAS, 260, 647

Hubeny, I., & Lanz, T. 1995, ApJ, 439, 875

Hubeny, I., Lanz, T., & Jeffery, C. S. 1994, Newsletter on Analysis of Astronomical Spectra (St Andrews Univ.), 20, 30

Hubeny, I. 1988, Comput. Phys. Commun., 52, 103

King, A. R. 1985, Nat, 313, 291

Knigge, C., Drake, N., Long, K. S., Horne, K., Wade, R. A., Baptista, R., Mauche, C. W., & Rutten, R. G. M. 1997, ApJ, in press

Kurucz, R. L., in Stellar Atmospheres: Beyond Classical Models, ed. L. Crivellari, I. Hubeny, & D. G. Hummer (Dordrecht: Kluwer), 441

Lomb, N. R. 1976, Ap&SS, 39, 447

Nather, R. E., & Robinson, E. L. 1974, ApJ, 190, 637

Nauenberg, M. 1972, ApJ, 175, 417

Paczyński, B., in Nonstationary Evolution of Close Binaries, ed. A. Zytkow (Warsa: Polish Sci. Publ.), 89

Patterson, J. 1981, ApJS, 45, 517

Petterson, J. 1980, ApJ, 241, 247

Ritter, H. 1990, A&AS, 85, 1179

Scargle, J. D. 1982, ApJ, 263, 835

Warner, B., & Nather, R. E. 1972, MNRAS, 159, 429

Warner, B., Cataclysmic Variable Stars (Cambridge: Cambridge University Press)

Zhang, E., Robinson, E. L., Stiening, R. F., & Horne, K. 1995, ApJ, 454, 447

TABLE 1. RESULTS OF MODEL FITS TO THE OSCILLATION SPECTRA

Spectrum	Run	Model	T (10^3 K)	A_{proj} [a] (A_{WD})	χ^2_ν [b] (N=263)
Pre-Eclipse	3	BB	>230	<0.004	1.10
$\phi_{orb} < 0.95$)	3	SA	>105	<0.02	1.13
	3	dB/dT	> 80		1.10
	4	BB	> 95	<0.01	0.95
	4	SA	> 85	<0.02	0.97
	4	dB/dT	> 50		0.95
Mid-Eclipse	3	BB	18^{+20}_{-5}	$0.05^{+0.12}_{-0.04}$	0.44
$(0.98 < \phi_{orb} < 1.02)$	3	SA	19^{+10}_{-4}	$0.07^{+0.04}_{-0.05}$	0.44
	3	dB/dT	13^{+6}_{-3}		0.44
	4	BB	28^{+145}_{-11}	$0.02^{+0.05}_{-0.019}$	0.41
	4	SA	26^{+114}_{-8}	$0.03^{+0.04}_{-0.028}$	0.41
	4	dB/dT	18^{+17}_{-5}		0.41
Post-Eclipse	3	BB	>110	<0.005	0.95
$(\phi_{orb} < 1.05)$	3	SA	> 85	<0.01	0.97
	3	dB/dT	> 60		0.95
	4	BB	>145	<0.003	1.29
	4	SA	> 95	<0.009	1.31
	4	dB/dT	> 65		1.29

Note.—Errors and lower limits are 2σ (95% confidence).

[a] A_{proj} is the projected area implied by the fit (in units of the WD surface area, $A_{WD} = 4\pi R^2_{WD}$) for an assumed distance of d=345 pc and $R_{WD} = 0.014 R_\odot$(Baptista et al. 1995).

[b] Where only lower limits on temperatures are given, the χ^2_ν values correspond to fits with $T_{eff} > 10^9$ K (BB and dB/dT models) or $T_{eff} > 1.4 \times 10^5$ K (SA models).